



RESEARCH ARTICLE

10.1029/2024MS004224

Special Collection:
Quantifying Nature-based
Climate Solutions

Key Points:

- We present a depth-averaged, dynamic Soil Model for Enhanced Weathering
- The model results are critically compared with four experimental data sets of different complexity
- The comparison demonstrates slower-than-expected dissolution rates

Supporting Information:

Supporting Information may be found in the online version of this article.

Correspondence to:

M. B. Bertagni,
matteo.bertagni@polito.it

Citation:

Bertagni, M. B., Calabrese, S., Cipolla, G., Noto, L. V., & Porporato, A. (2025). Advancing enhanced weathering modeling in soils: Critical comparison with experimental data. *Journal of Advances in Modeling Earth Systems*, 17, e2024MS004224. <https://doi.org/10.1029/2024MS004224>

Received 10 JAN 2024




Accepted 25 NOV 2024

Corrected 21 APR 2025

This article was corrected on 21 APR 2025. See the end of the full text for details.

© 2024 The Author(s). Journal of Advances in Modeling Earth Systems published by Wiley Periodicals LLC on behalf of American Geophysical Union. This is an open access article under the terms of the [Creative Commons Attribution-NonCommercial-NoDerivs License](#), which permits use and distribution in any medium, provided the original work is properly cited, the use is non-commercial and no modifications or adaptations are made.

Advancing Enhanced Weathering Modeling in Soils: Critical Comparison With Experimental Data

Matteo B. Bertagni^{1,2,3} , Salvatore Calabrese⁴, Giuseppe Cipolla⁵, Leonardo V. Noto⁵ , and Amilcare Porporato^{2,3} 

¹Department of Environment, Land and Infrastructure Engineering, Politecnico di Torino, Torino, Italy, ²The High Meadows Environmental Institute, Princeton University, Princeton, NJ, USA, ³Department of Civil and Environmental Engineering, Princeton University, Princeton, NJ, USA, ⁴Department of Biological and Agricultural Engineering, Texas A&M University, College Station, TX, USA, ⁵Dipartimento di Ingegneria, Università degli Studi di Palermo, Palermo, Italia

Abstract Enhanced weathering (EW) is a promising strategy to remove atmospheric CO₂ by amending agricultural and forestry soils with ground silicate rocks. However, current model-based EW assessments face large uncertainties stemming from the intricate interplay among soil processes, compounded by the absence of a detailed comparison with available observational data. Here, we address this critical gap by first advancing a dynamic, ecohydrological, and biogeochemical Soil Model for Enhanced Weathering (SMEW). We then conduct a hierarchical model-experiment comparison with four experimental data sets of increasing complexity, from simple closed incubation systems to open mesocosm experiments. The comparison demonstrates SMEW's ability to capture the dynamics of primary variables, including soil moisture, alkalinity, and inorganic carbon. The comparison also reveals that weathering rates are consistently lower than traditionally assumed by up to two orders of magnitude. We finally discuss the implications for carbon removal scenarios and avenues for further theoretical and experimental explorations.

Plain Language Summary Enhanced weathering (EW) is a promising strategy to mitigate climate change while increasing agricultural productivity and mitigating ocean acidification. The strategy involves amending cropland and forest soils with finely ground silicate rocks, which sequester atmospheric CO₂ upon dissolution. However, current EW assessments relying on models face uncertainty, primarily stemming from challenges in accurately representing the intricate hydrological and biogeochemical processes driving mineral dissolution in the soil. The absence of a robust model-data comparison exacerbates these uncertainties. This study addresses these issues by presenting a model for EW dynamics in the upper soil layer, successfully replicating diverse experimental data sets. Our model reveals a slower mineral dissolution than conventionally assumed, offering insights into EW potential as a negative emission strategy.

1. Introduction

In addition to emissions reduction from every sector, significant carbon dioxide removal (CDR) through negative emission technologies (NETs) is needed to limit global warming (Calvin et al., 2023). Among various proposed NETs, enhanced weathering (EW) is emerging as one with considerable CO₂ removal potential and low technological requirements (Beerling et al., 2020; Berge et al., 2012; Calabrese et al., 2022; Hartmann et al., 2013; Kohler et al., 2010; Renforth, 2012; Taylor et al., 2016). EW relies on amending agricultural and forestry soils with crushed silicate materials (e.g., basalt, dunite, wollastonite) to promote biomass growth and sequester CO₂ in aqueous or mineral forms (Hartmann et al., 2013; Taylor et al., 2021). Upon dissolution, the hydrologic cycle transports part of the EW products to surface freshwaters and the ocean, mitigating ocean acidification and stably sequestering atmospheric CO₂ for geological timescales (Bertagni & Porporato, 2022; Renforth & Henderson, 2017). As a further co-benefit, EW is expected to improve nitrogen use efficiency in agricultural fields, reducing reactive nitrogen emissions and the demand for fossil-fuel-based fertilizers (Blanc-Betes et al., 2021; Val Martin et al., 2023). Deployed over suitable lands at the global scale, it is estimated that EW potential may reach the order of gigatonnes of CO₂ removal per year (Baek et al., 2023; Beerling et al., 2020; Streffer et al., 2018; Taylor et al., 2016).

Despite these promising estimates, EW assessments face significant uncertainties rooted in the complex interplay between hydrological and biogeochemical processes across scales (Calabrese et al., 2022). Weathering rates

exhibit considerable variability, spanning orders of magnitudes due to rock specifics, and temporal and spatial heterogeneity in hydroclimatic drivers and soil processes (Deng et al., 2022; Jung & Navarre-Sitchler, 2018; Li et al., 2022; Schabernack & Fischer, 2022). This variability complicates efforts to reconcile theoretical expectations with laboratory observations, even for the same rock type (Amann et al., 2020; Buckingham et al., 2022; Renforth et al., 2015). Field trials are in their nascent stages, and monitoring, reporting, and verifying CDR in open, heterogeneous, and multiphase soil systems face inherent challenges (Clarkson et al., 2023), although recent efforts have started to address them (Amann & Hartmann, 2022; Knapp et al., 2023; Reershemius et al., 2023). Specifically, soil-based mass balance approaches, initially used for natural chemical weathering but modified to reduce analytical error, could be a promising option to resolve the small signal-to-noise ratios in EW mineral cation depletion (Reershemius et al., 2023). When EW is applied to significant portions of a watershed area, stream water chemistry analyses may also be beneficial to understand the transport of the mineral dissolution products (Larkin et al., 2022), as in the case of agricultural liming (Hamilton et al., 2007). Quantifying this transport from the field to CO₂ storage locations, such as deep aquifers or the oceans, is a crucial and yet largely unexplored EW aspect (Bertagni & Porporato, 2022; Bertagni et al., 2024; Calabrese et al., 2022; Hartmann et al., 2013; Zhang et al., 2022).

Within this intricate context, current estimates of EW potential as a NET heavily rely on models, mostly vertically explicit reactive transport models, where minerals added to the topsoil layers undergo dissolution based on transition state theory (Baek et al., 2023; Beerling et al., 2020; Kantzas et al., 2022; Taylor et al., 2016). While these models can comprehensively treat reacting chemical species across a heterogeneous soil profile, they are usually used under simplifying assumptions, such as constant vertical water flow and homogeneous soil properties. An alternative, spatially lumped approach focuses on the temporal dynamics of average quantities within the upper soil layers—the most dynamic soil layers, where ground rocks are introduced—hence emphasizing temporal over spatial variability (Cipolla et al., 2021a, 2021b). Given the direct and indirect impacts of hydroclimate conditions and soil moisture dynamics on weathering rates, capturing temporal variability is crucial. Soil moisture influences the surface area of EW material in contact with water and the dilution and leaching of weathering products. Moreover, it affects biotic and abiotic soil processes influencing EW dynamics, including carbon cycling, bacterial activity, and solute, heat, and gas transfers (Manzoni et al., 2012; Miele et al., 2023; Porporato & Yin, 2022).

Surprisingly, despite numerous experimental works in the last decade (Amann et al., 2020; Buckingham et al., 2022; Dietzen et al., 2018; Kelland et al., 2020; Renforth et al., 2015; te Pas et al., 2023; Vienne et al., 2022), comparisons of model results with experimental observations have been minimal (Kelland et al., 2020). An extensive model-data comparison is hence pivotal, not only to validate EW models for realistic assessments of net-zero scenarios but also to improve modeling assumptions, provide a hypothesis-testing tool to investigate EW processes, design better experiments, and quantify uncertainty.

Our work addresses this gap, presenting an ecohydrological and biogeochemical Soil Model for EW (SMEW) and using the model for an extensive and systematic model-experiment comparison. Specifically, the model is a substantial evolution of the model initially conceived by Cipolla et al. (2021a), including several improvements in model closures and additions of new model components (Section 2). The model performance is compared with four experimental data sets covering a gradient of complexity, from simple closed incubation systems to more complicated, open mesocosm experiments (Section 3). The model-data comparison demonstrates that the model captures the dynamics of the primary variables of interest and provides crucial insights into weathering rates (Section 4). We finally identify model limitations and discuss areas requiring further theoretical and experimental exploration.

2. Soil Model for Enhanced Weathering

This model builds upon prior work on EW in the soil's upper layers (Cipolla et al., 2021a, 2021b) incorporating several extensions and improvements in model closures and new model components. The model emphasizes the dynamic behavior of depth-averaged quantities within the upper soil layers. The depth-averaged approach is especially appropriate when agricultural practices have homogenized the upper soil layers (Porporato & Yin, 2022). The critical components of the model revolve around the intricate interplay between the water balance, influenced by stochastic infiltration rates, and the biogeochemical processes occurring within the multiphase soil porous media. Figure 1 provides an overview of the main model components. In this section, we discuss the mass

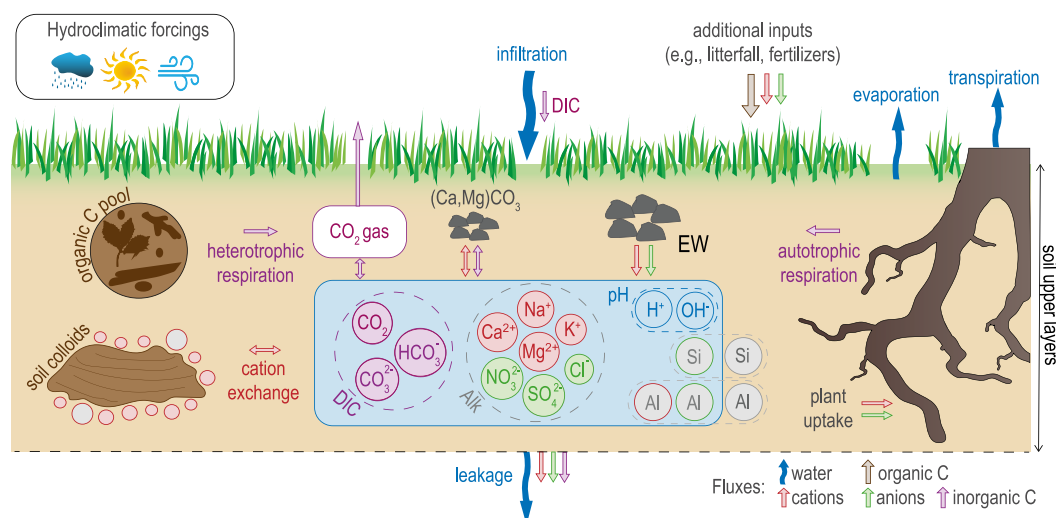


Figure 1. Sketch of the biogeochemical and ecohydrological processes represented in the Soil Model for Enhanced Weathering (SMEW). SMEW is a dynamic, depth-averaged model for the upper soil layers where the crushed rock is applied.

balances for the key variables of interest, which form a dynamic system of ordinary differential equations (ODEs). Jointly with the ODE system, we solve a set of algebraic equations based on a quasi-steady-state approximation to account for aqueous carbon and aluminum speciation and the cation redistribution between adsorbed and dissolved phases (Appendix A). The dynamics of plants and their roles in EW are presented in Appendix B. A discussion of the model parameters is reported in the Supporting Information (Text S1 in Supporting Information S1).

2.1. Hydroclimate and Moisture Dynamics

Hydroclimatic forcings such as temperature and rainfall exert critical controls on weathering rates (Calabrese & Porporato, 2020; Deng et al., 2022) by directly influencing water availability and distribution, mineral dissolution kinetics, and impacting various biogeochemical processes, including biotic activity and chemical equilibria. In SMEW, these hydroclimatic factors can be introduced through observational or reanalysis data or generated through modeling for future projections. Of particular significance to the correct representations of weathering dynamics are the short-term hydrological fluctuations because of their nonlinear feedback on soil hydro-biogeochemistry (Cipolla et al., 2021a; Dong et al., 2023; Laio et al., 2001; Porporato, D'Odorico, et al., 2003; Porporato & Yin, 2022). Consequently, our modeling framework incorporates a water mass balance reproducing the time (t) evolution of relative soil moisture (s) within the soil depth (Z)

$$nZ \frac{ds}{dt} = R(t) - Q(s, t) - E(s) - T(s) - L(s), \quad (1)$$

where n is soil porosity, $R(t)$ is rainfall, $Q(s, t)$ is runoff, $E(s)$ is evaporation, $T(s)$ is plant transpiration, and $L(s)$ is leaching. In the absence of data, rainfall can be modeled as a stochastic marked Poisson process (Porporato & Yin, 2022; Rodríguez-Iturbe et al., 1999). Surface runoff, resembling Horton overland flow, is activated when the rainfall exceeds the available storage capacity. Evaporation and transpiration fluxes are influenced by soil moisture and vegetation cover (Laio et al., 2001), and their cumulative effect is bounded by the potential evapotranspiration (ET_0), which can be estimated using the Penman-Monteith method for a reference crop, based on climatic conditions such as temperature, wind speed, latitude, and albedo (Allen et al., 1998). Water leakages to lower soil horizons are modeled as a power law of soil moisture with coefficients depending on soil texture (Laio et al., 2001).

2.2. Organic Carbon and Heterotrophic Respiration

In the topsoil layers, soil carbon exists in organic and inorganic forms. The flux from organic to inorganic carbon pools results from the decomposition of soil organic matter, mostly driven by biotic processes like bacterial

activity. This flux, called heterotrophic soil respiration, is a key contributor to elevated CO₂ levels in soil air, making it a critical factor in the potential EW efficiency in soil carbon sequestration. To model the dynamics of organic carbon (OC), here considered as dead biotic material, we employ a simple balance that includes an addition term (ADD), accounting for inputs like litterfall or soil amendments, and a decomposition term (DEC) representing biotic activity (Cipolla et al., 2021a; Porporato, D'Odorico, et al., 2003). The mass balance for OC is

$$\frac{dOC}{dt} = \text{ADD} - \text{DEC}. \quad (2)$$

Depending on the available information, the addition of OC can be assumed to be constant, vary seasonally, or be based on photosynthetic activity. The decomposition term is proportional to the available OC through a moisture- and temperature-dependent coefficient (Cipolla et al., 2021a; Porporato, D'Odorico, et al., 2003). A fraction r of the decomposed OC is converted into inorganic carbon, defining soil heterotrophic respiration ($\text{RESP}_h = r \text{ DEC}$). The remaining fraction $(1 - r)$ is assumed to be converted into living biomass of soil biota (e.g., bacteria, fungi, and soil fauna), which is not explicitly modeled (Porporato, Laio, et al., 2003). While here we use a minimalist soil OC model, more elaborate representations of the OC cycle (e.g., with explicit microbial dynamics) may be adopted (Jha et al., 2023; Wieder et al., 2013) based on specific scientific questions being addressed in the interactions between OC and EW.

2.3. Inorganic Carbon Pools

The negative-emission potential of enhanced weathering hinges on the sequestration of inorganic carbon, mainly in the form of aqueous carbonates within soil water and throughout the hydrological cycle, or through the formation of secondary carbonate minerals, albeit with a 50% reduction in CO₂ removal efficiency (Bertagni & Porporato, 2022; Hartmann et al., 2013). The main components of soil inorganic carbon include CO₂ in the soil air phase, dissolved inorganic carbon (DIC) in the soil water, and carbon stored in mineral forms. Given that the equilibration timescale of aqueous and gaseous forms is much faster than that of carbonate mineral precipitation and dissolution, we consider two distinct inorganic carbon pools: one that combines aqueous and gaseous forms (IC) and another accounting for mineral inorganic carbon (MIC). The overall mass balances for IC and MIC are expressed as:

$$\frac{dIC}{dt} = \text{RESP}_{h+a} + I_w \cdot [\text{DIC}]_{I_w} - L \cdot [\text{DIC}] - F_{\text{ADV+DIFF}} + W_{(\text{Ca,Mg})\text{CO}_3}, \quad (3)$$

$$\frac{dMIC}{dt} = -W_{(\text{Ca,Mg})\text{CO}_3}, \quad (4)$$

where $[\cdot]$ indicates concentration. RESP_{h+a} is the sum of heterotrophic and autotrophic respiration, respectively. Autotrophic respiration (RESP_a), namely the release of CO₂ gas by plant roots, is estimated to scale with vegetation (Appendix B) and to be equivalent to heterotrophic respiration (Section 2.2) when plants are fully grown (Bond-Lamberty et al., 2004). Another minor source of inorganic carbon in the soil is the DIC in infiltrating water ($I_w = R - Q$). IC can exit the control volume as aqueous DIC through leaching ($L \cdot [\text{DIC}]$) or as gaseous CO₂ to the atmosphere through diffusive or advective fluxes ($F_{\text{ADV+DIFF}}$) (Cipolla et al., 2021a; Millington & Quirk, 1961). The term $W_{(\text{Ca,Mg})\text{CO}_3}$ accounts for the dissolution (>0) or precipitation (<0) of calcium and magnesium carbonates, modeled following Kirk et al. (2015). The redistribution of IC between soil air CO₂ and aqueous carbonates follows equilibrium assumptions (Appendix A).

2.4. Biogeochemistry of Alkaline and Acid Elements

To promote inorganic carbon sequestration, EW aims to release alkaline cations (Ca²⁺, Mg²⁺, K⁺, Na⁺) in soil water and throughout the hydrological cycle (Hartmann et al., 2013). These cations increase water alkalinity and promote a transfer of CO₂ from the atmosphere to the water by forming aqueous carbonates in favorable water-chemistry conditions (Bertagni & Porporato, 2022). We hence consider four mass balances for each of these alkaline cations, indicated generically as X. The mass balances for any total cation content (X_{tot}) within the control volume, comprising cations dissolved in the soil solution and those adsorbed onto soil colloids, can be written as

$$\frac{dX_{\text{tot}}}{dt} = I_X + EW_X + W_{X\text{CO}_3} - (L + T)[X] - UP_X. \quad (5)$$

I_X accounts for background cation inputs like litterfall decomposition, fertilizer addition, and background weathering processes. EW_X denotes the cation release by the EW application, and $W_{X\text{CO}_3}$ is the release from the weathering of Ca or Mg carbonate. The term $(L + T)[X]$ characterizes the outflow resulting from leaching and plant passive uptake, while UP_X pertains to active plant uptake during growth (Appendix B). Given the total cation amount in the control volume, the partitioning between adsorbed and aqueous components follows equilibrium assumptions (Appendix A).

A similar mass balance approach applies to the major strong anions commonly found in soil solutions (e.g., Cl^- , NO_3^{2-} , SO_4^{2-}) that do not undergo speciation at pH values of interest. Conveniently, we do not need to discriminate between the various anions of the strong acids because (a) EW aims to increase cation concentrations, (b) anion adsorption is mostly negligible in many soil environments, (c) it is the cumulative presence of these anions that defines soil water alkalinity (Appendix A). We can thus collectively denote these anions as An and write a single mass balance

$$\frac{d\text{An}_{\text{tot}}}{dt} = I_{\text{An}} - (L + T)[\text{An}], \quad (6)$$

where I_{An} signifies background anion input, and $(L + T)[\text{An}]$ represents anion losses due to leakages and passive plant uptake. More granular representations of the anion pools can be adopted depending on the specific scientific questions being addressed (e.g., nitrogen cycling).

2.5. Silicon and Aluminum Balances

Since the most promising options for large-scale EW applications are silicate minerals and rocks, EW is anticipated to release large amounts of silicon (Si) into soils. This constitutes a potential EW co-benefit, as soil Si is a biotic nutrient that enhances plants' immune system (Fauteux et al., 2005; Kim et al., 2014), although the overall effect on soil properties (e.g., hydraulic conductivity) is largely unknown. Soil Si chemistry is rather complex, comprising dissolved species, amorphous solid phases, and organic and inorganic complexes (Schaller et al., 2021), and its dynamics is expected to impact soil formation processes on long timescales (Weil & Brady, 2016). Given that the impact of Si on the CO_2 sequestration dynamics by EW is minor, here we follow a simplified approach, wherein we consider Si as dissolved silicic acid. More complex mass balances could be adopted depending on the goal of the investigation. The mass balance hence is

$$\frac{d\text{Si}_{\text{tot}}}{dt} = I_{\text{Si}} + EW_{\text{Si}} - (L + T)[\text{Si}] - UP_{\text{Si}}, \quad (7)$$

where I_{Si} represents background Si inputs, EW_{Si} accounts for Si released through EW applications, $(L + T)[\text{Si}]$ signifies Si outflow due to leaching and passive plant uptake, and UP_{Si} denotes active plant uptake during growth.

Aluminum is a prevalent element in highly weathered, acidic soils, where it can be found in complexes, in the soil solution, or as cations adsorbed into soil colloids. In acidic conditions, aluminum plays a crucial role as a buffering agent but can be toxic to soil biotic activity and plants in high concentrations (Weil & Brady, 2016). Although Al is an undesired product, EW applications may release some of it, depending on the mineral composition of the rock applied. The mass balance for aluminum is expressed as

$$\frac{d\text{Al}_{\text{tot}}}{dt} = I_{\text{Al}} + EW_{\text{Al}} - L[\text{Al}_{\text{mob}}], \quad (8)$$

where I_{Al} and EW_{Al} correspond to background and EW-induced Al releases, respectively. Aluminum losses are assumed to occur solely through the leaching of Al's more soluble and mobile forms ($[\text{Al}_{\text{mob}}]$), which can be abundant in highly acidic (pH < 4.5) or alkaline (pH > 7) conditions. Aluminum speciation reactions are reported in Appendix A.

2.6. Rock Weathering

Modeling rock weathering is pivotal to understanding and quantifying EW dynamics and temporal efficiency. Applied rocks are typically composed of various minerals, and the release of a specific element like an alkaline cation X (Section 2.4) results from the collective contribution of mineral dissolution. This contribution depends on the mineral dissolution rate (W_i) and the mineral surface area (SA_i), and can be expressed as

$$EW_X = \sum_i m_{X,i} \cdot SA_i \cdot W_i(s, \Theta, \text{pH}) \quad (9)$$

where $m_{X,i}$ accounts for the stoichiometry of the element X in the mineral i , and Θ stands for temperature. The same equations, with coefficients $m_{Al,i}$ and $m_{Si,i}$, apply to the release of Al and Si, namely EW_{Al} and EW_{Si} in Equations 7 and 8. The mineral surface area SA_i is determined according to the methodology proposed by Beerling et al. (2020), which accounts for the dynamically evolving rock composition and particle size distribution and the fractal dimension of the particle surface.

For the weathering rates, we follow previous EW modeling efforts (Beerling et al., 2020; Kanzaki et al., 2022; Taylor et al., 2016) and use the semi-empirical formula by Palandri (2004). This seminal formulation, stemming from the work of Lasaga (1984), is based on dissolution experiments in stirred reactors without diffusive limitations and under conditions far from equilibrium. The formula accounts for the most well-studied mechanisms of mineral dissolution, driven by the water species H_2O , H^+ , and OH^- . As previously implemented by Cipolla et al. (2021a), we also consider the dependence of mineral dissolution rates on the relative soil moisture value (s) to account for the wet portion of the mineral surface that can actually undergo dissolution. The formula for the weathering rate of each mineral can thus be expressed as:

$$W_i = F_D \cdot s \cdot \sum_j k_{i,j}(\Theta) \cdot a_j^{n_{i,j}} \cdot (1 - \Omega_i^{p_{i,j}})^{q_{i,j}}, \quad (10)$$

where j is the individual weathering agent (H_2O , H^+ , OH^-) and a_j are the agent activities (here approximated as concentrations). $k_{i,j}(\Theta)$ are the mineral- and agent-dependent rates accounting for temperature (Θ) effects, and $n_{i,j}$ are the reaction order constants (Palandri, 2004). Ω_i is the mineral saturation index (Morel & Hering, 1993). The coefficients $p_{i,j}$ and $q_{i,j}$ have been quantified only for very few minerals and agents and are approximated to unity (Palandri, 2004). F_D is a dissolution factor representing possible inhibition ($F_D < 1$) or enhancement ($F_D > 1$) of weathering rates, similar to the coefficients used in previous natural weathering studies (Maher et al., 2009). For the model-experiment comparison, we will quantify F_D with experimental observations. As later discussed (Section 4.1), the observation-driven quantification of F_D is crucial to assess actual weathering rates and the validity of Palandri's formulation in the soil environment.

2.7. Model Setup and Simulation Example

The model requires a characterization of the hydroclimatic forcings, the EW material and application rate, the plant, and the soil biophysical properties. Rainfall and temperature are key hydroclimatic forcings that impact virtually all model components. Wind speed and albedo play a role in influencing potential evapotranspiration (Allen et al., 1998). For EW application, details include the amount and mineral composition of the applied rock, particle size distribution, and specific surface area. Plant characterization involves parameters like carrying capacity, growth rate, and root area index, measured or derived from the literature (Appendix B). Soil characterization requires details on soil texture, initial OC content and pH, and inorganic chemistry. Notably, assuming a quasi-steady state equilibrium of the soil chemistry allows constraining the air-water carbonate system using a single quantity (e.g., the CO_2 partial pressure) in addition to the soil pH (Stumm & Morgan, 1996). For the biogeochemistry of the major ions, minimum initial data requires either the adsorbed fractions on the cation exchange capacity (CEC), the concentrations in the soil solution, or the total quantities per unit of soil. The others are determined through the Gaines-Thomas convention (Appendix A). In the absence of specific data, background elemental input fluxes, for example, I_X in Equation 5, can be defined to balance background losses, for example, $[x]_{\text{initial}}(\bar{T} + \bar{L})$ here the bar denotes temporal averaging. This approach ensures that the initial condition represents a long-term average state of the soil that is reestablished whenever the EW application is absent or concluded.

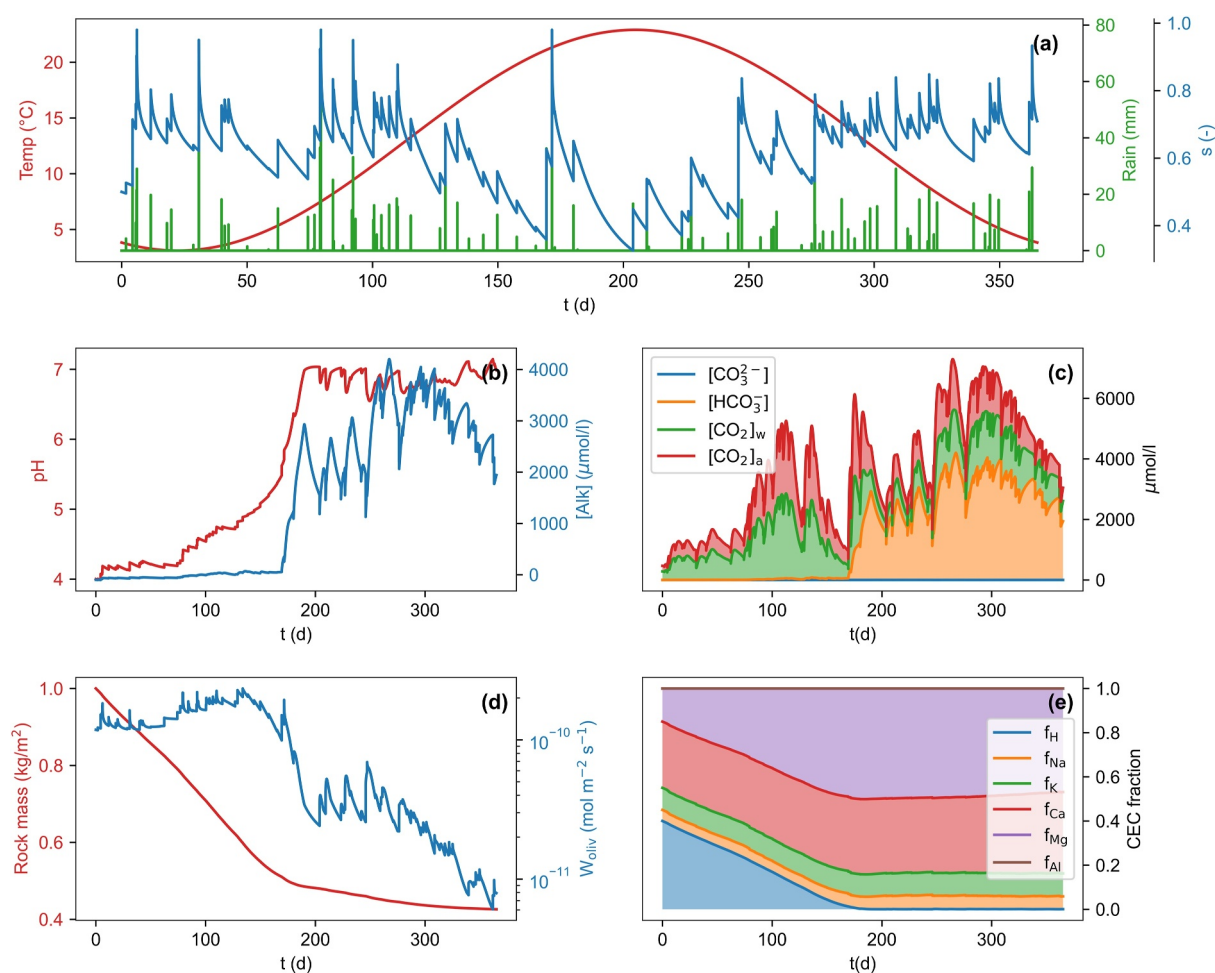


Figure 2. Example of model output for an Enhanced weathering application (1 kg/m²) with forsterite (Mg₂SiO₄) in a temperate humid climate ($F_D = 1$). (a) Temperature, rainfall, and soil moisture. (b) Soil water pH and alkalinity. (c) Inorganic carbon speciation. (d) Mineral mass and weathering rate. (e) Soil cation adsorption. Simulation results extended to 10 and 50 years are reported in Figures S1 and S2 in Supporting Information S1. A baseline simulation without the rock application is reported in Figure S3 in Supporting Information S1.

Figure 2 shows an example of a 1-year simulation for a 1 kg/m² (10 tonn/ha) EW application with forsterite (Mg₂SiO₄) in a temperate humid climate. Longer simulations of 10 and 50 years showing the long-term impact of mineral dissolution are reported in Figures S1 and S2 in Supporting Information S1. A baseline simulation without rock application is reported in Figure S3 in Supporting Information S1. The mean temperature is 13°C, and the yearly cumulative rainfall is 1,200 mm. The simulated soil is an organic-rich (initial OC is 5%) and acidic (initial pH is 4) loam. Results show how the low soil pH favors the mineral dissolution rate but impedes the formation of aqueous bicarbonates in the soil solution for the first 170 days. The trend reverses when the pH gets around 6, with slower dissolution rates and bicarbonate formation. This trade-off between mineral dissolution kinetics and CO₂ sequestration efficiency has been previously explored (Bertagni & Porporato, 2022). Additionally, as the pH rises, the CEC base saturation increases, with Mg²⁺ replacing the acid ion H⁺ (panel e), highlighting the potential of EW for liming purposes.

3. Comparison With Experiments

This section compares the model outcomes with available experimental data. Specifically, we use four different experimental data sets derived from experiments conducted at varying levels of complexity: (a) small-scale vials open to the atmosphere and with moist acidic soils (Dietzen et al., 2018); (b) small down-flow soil columns open to the atmosphere and water leaching (te Pas et al., 2023); (c) two more complete mesocosm experiments incorporating growing vegetation (Amann et al., 2020; Kelland et al., 2020). The comparison with these different

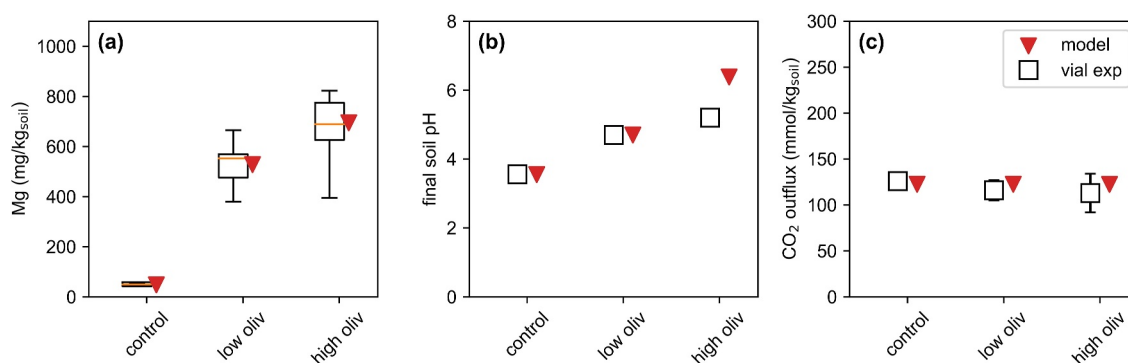


Figure 3. Model-experiment comparison based on the vial experiments by Dietzen et al. (2018). (a) Final Mg accumulation in the soil. For the experimental replicates (10 for each case), the central line represents the median value, the boxes span from the 25th to 75th percentiles, and the whiskers extend from the minimum to the maximum value. (b) Final soil pH (c) Mean cumulative net CO₂ flux to the atmosphere, showing minimal variations across treatments. Error bars indicate experimental standard deviation (SD)—not shown if shorter than the symbol size.

experimental setups gives the advantages of compartmental investigations of the model performance and a broad examination of EW dynamics under different environmental forcings. Because our model is spatially lumped and designed for the upper soil layers, we preferred not to include experiments conducted with vertically deep and heterogeneous soil cores (Buckingham et al., 2022; Renforth et al., 2015; Vienne et al., 2022). A summary of the model set-up based on available experimental information is provided in Table S1 in the Supporting Information.

3.1. Acidic Soil in Vials

Our first comparison involves the experiments by Dietzen et al. (2018), which entailed a 3-month soil incubation study to assess the weathering of olivine (mainly composed of forsterite, Mg₂SiO₄) and its impact on available Mg levels, pH, and soil CO₂ flux. The experiments employed 110 ml open vials filled with soil that remained consistently moist throughout the study. Olivine was added at varying application rates. The open vials allowed CO₂ exchange with the atmosphere while preventing downstream water leaching. Although these experiments simplified the soil environment considerably, they provided valuable insights by enabling a direct assessment of the soil-water-air chemistry influenced by the mineral dissolution.

We conducted model simulations, configuring the numerical parameters to align with the experimental conditions (Table S1). The sandy soil was characterized by high acidity (initial pH = 3.55) and substantial OC content (initial OC = 5.5%). Olivine powder with an average diameter of 20 μm was applied at two distinct rates, equivalent to 1 and 5 kg/m². The soil was constantly moist, and the temperature was fixed at the experimental value of 22°C. The initial CO₂ concentration in the soil air was set at 23 times atmospheric values to reproduce the observed soil respiration flux. Data about adsorbed species were not provided in the experimental work, so we estimated a CEC of 10 cmol_c/kg_{soil} with 10% base saturation from literature values for extremely acidic sandy loam (Weil & Brady, 2016). Different assumptions on the CEC and its base saturation have little quantitative impact on the results (Figures S4 and S5 in Supporting Information S1). The simulations encompass the three experimental scenarios: control, and low and high olivine applications.

The comparison between simulations and experiments is presented in Figure 3, which highlights the Mg accumulation in the vial due to mineral dissolution (a), the soil pH shifts (b), and the flux of CO₂ from the soil to the atmosphere (c). The simulations closely align with the experimental findings in all three scenarios. Notably, the Mg accumulations in the vials constrain the weathering rates since there are no Mg losses from the control volume. As further commented in the discussion (Section 4.1), the dissolution factor F_D in the weathering Formula 10 had to be adjusted to values $\mathcal{O}(0.1)$, implying that Palandri's Formula 10 substantially overestimated the mineral dissolution rate. The pH shifts show good agreement except in the high-olivine application, suggesting that experimental soil pH is more buffered than what our numerical simulations reproduce, possibly due to the assumed CEC (Figure S5 in Supporting Information S1). The CO₂ flux to the atmosphere remains nearly identical in the control and olivine treatments, implying limited CO₂ sequestration in either experiment or model. This is due to the low pH levels that impede aqueous carbonate formation (Bertagni & Porporato, 2022; Dietzen &

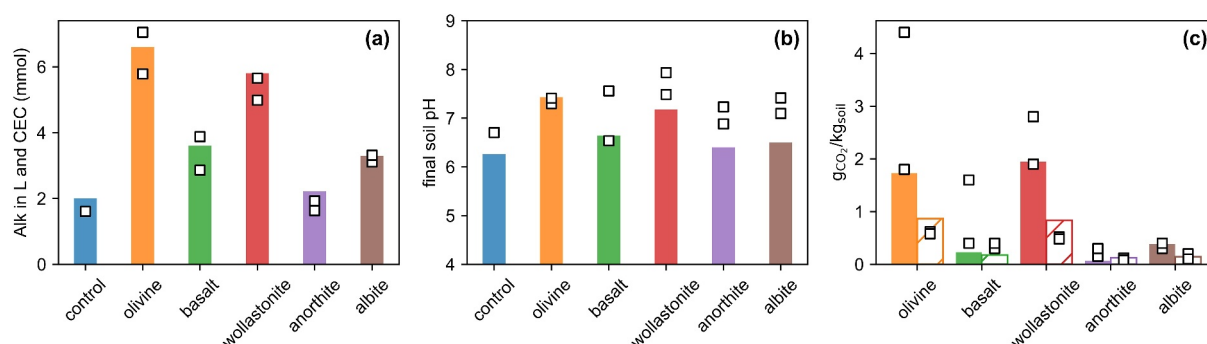


Figure 4. Model-experiment comparison based on the down-flow bottle experiments by te Pas et al. (2023). Square symbols stand for the experimental replicates. (a) Total alkalinity observed in the leaching and on the cation exchange capacity. (b) Final soil pH. (c) Potential (filled bars) and effective (dashed bars) CO_2 sequestration. The difference is due to alkalinity adsorption on the cation-exchange sites.

Rosing, 2023). More extended experiments allowing for further olivine dissolution would raise the pH to favorable values for CO_2 sequestration.

3.2. Soil Columns With Leaching

Our second comparison is with experiments conducted by te Pas et al. (2023), featuring small down-flow soil columns of 180 ml polyethylene containers. These columns were equipped with perforated bases to enable water leaching. The experiments thus account for a rudimentary hydrologic cycle, wherein the soil-rock mixture undergoes wet-dry cycles with water added every 3 days. A further advantage of these 9-week experiments is that they assessed the EW potential of five distinct rocks and minerals: forsterite (Mg_2SiO_4), wollastonite (CaSiO_3), anorthite ($\text{CaAl}_2\text{Si}_2\text{O}_8$), albite ($\text{NaAlSi}_3\text{O}_8$), and basalt.

We conducted model simulations utilizing parameters directly derived from the experiments. The sandy soil had an initial pH of 5.2 and an OC content of 2.1%. Deterministic rainfall events of constant intensity were applied at 3-day intervals with deionized water (no alkalinity inputs). The resulting rainfall regime (around 3,200 mm/yr) is typical of tropical regions. Rock powder application mirrored the experimental high load of 12.5 kg/m² across all cases, incorporating different particle size distributions and specific surface areas. Albite mineral composition included a 3% of wollastonite. Without data regarding the mineral composition of basalt, we adopted the basalt characterization from Beerling et al. (2020). The temperature was set at 22°C. Equilibrium-based initial conditions for adsorbed and dissolved species were established based on experimental measurements of total alkaline cation (Ca, Mg, K, Na) quantities. The CEC was fixed at the effective CEC value (3 cmol_c/kg_{soil}) observed at the beginning of the experiments.

Figure 4 presents the model-experiment comparisons for the total alkalinity release by mineral dissolution (a), the increase in soil pH (b), and the CO_2 captured by the EW applications (c). The total alkalinity release includes alkalinity observed in leaching and soil adsorption (see Figure S6 in Supporting Information S1 for the partitioning between the two phases) and constrains the mineral weathering rates, giving F_D values in the weathering Formula 10 consistently below one. The pH shifts show a reasonable agreement, although the numerical simulations do not fully reproduce the increase in pH that is observed experimentally. This is consistent with the observed experimental increase in soil pH in the absence of rock application, which the model only partially reproduces. The pH temporal dynamics (Figure S6 in Supporting Information S1) further reveal a model-experiment difference in the first days of the experiment, where the model does not reproduce the pH experimental drop likely driven by the acidity released by the cation exchange. Following the experimental work (te Pas et al., 2023), we quantified the CO_2 sequestration in two ways: one based on the alkalinity liberated through rock dissolution (potential CO_2 sequestration) and the other accounting for aqueous carbonate leaching and additional inorganic carbon stored in the soil (effective CO_2 capture). The difference between the potential and effective CO_2 sequestration is due to the alkalinity adsorption on cation-exchange sites, which does not promote aqueous carbonate formation. Consistently with the experiments, the effective CO_2 sequestration is significantly lower than the potential CO_2 sequestration across all experiments.

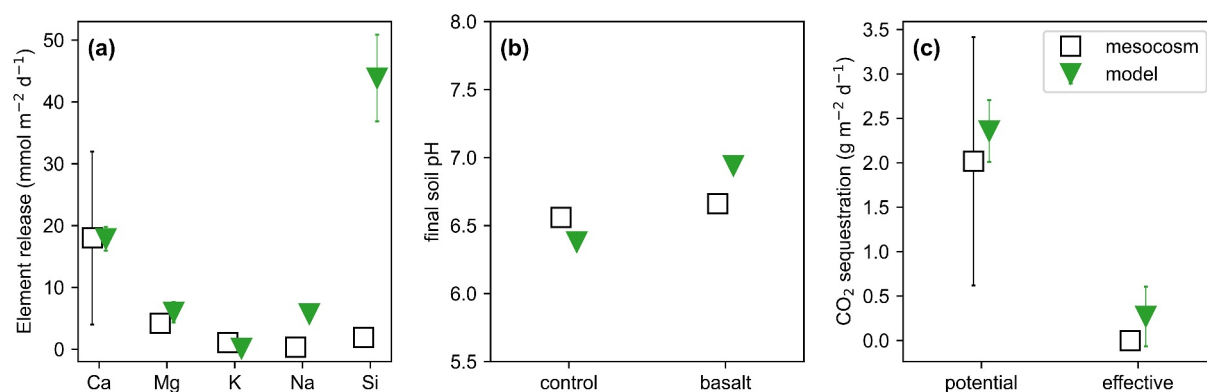


Figure 5. Model-experiment comparison based on the mesocosm experiments by Kelland et al. (2020). (a) Daily averaged elemental release of basalt dissolution per land surface unit, with bars in model results indicating ± 1 SD associated with time variability. (b) Final pH. (c) Potential (alkalinity release) and effective (aqueous carbonate leaching) CO₂ sequestration.

3.3. Mesocosms With Vegetation

The third and fourth comparisons are with mesocosm experiments (Amann et al., 2020; Kelland et al., 2020). A distinctive feature of these experiments was the inclusion of actively growing vegetation, specifically sorghum in Kelland et al. (2020) and wheat and barley in Amann et al. (2020). Vegetation introduces complexities to soil hydrology and biogeochemistry through water transpiration, nutrient uptake, and CO₂ autotrophic respiration (Appendix B). Although the representation of the hydrological cycle in these experiments remained somewhat simplified with periodic (1–7 days) and fixed amounts of water addition, the dynamic interplay with vegetation growth resulted in notable water flux shifts during the growing season. This allowed for an expanded comparative analysis, including examining hydrological and soil biogeochemical processes.

3.3.1. Reactor Columns

Kelland et al. (2020) conducted experiments in reactor columns measuring 16 cm in diameter and 50 cm in depth over 120 days. We ran model simulations based on the experimentally observed parameters as in the previous comparisons. The soil was classified as a clay loam with an initial pH of 6.6 and an OC content of 1.2%. The simulations incorporated a rainfall regime typical of temperate humid and tropical regions (about 2,000 mm/yr), with water added every 5 days. To estimate the potential evapotranspiration, we numerically recreated the experimental artificial day. This involved maintaining photosynthetically active radiation (800 $\mu\text{mol photons m}^{-2} \text{s}^{-1}$) for 18 hr during the initial 60 days and 10 hr for the subsequent 60 days. Daily temperatures were computed by temporally averaging the 25 and 17°C of the artificial day and night, respectively. We used experimental values for the basalt application (high load of 10 kg/m²), rock mineral composition, specific surface area, and particle size distribution. Due to the depth-averaged model framework, we could not reproduce the experimental vertical heterogeneity, with basal being mixed only in the first 25 cm of the soil column. The CEC was fixed at the experimental value of 25 cmol_c/kg_{soil}, and the initial saturation fractions were estimated based on the cation concentrations measured in the leachate of the untreated experiment.

Figure 5 presents the model-experiment comparison for the elemental release through basalt dissolution (a), the impact on soil pH (b), and potential and effective CO₂ sequestration (c). The model captures well the release of alkaline nutrients Ca, Mg, and K. We stress, however, that the very fast dissolution of apatite, Ca₅(PO₄)₃(OH), comprising around 3% of the basalt, could not be numerically reproduced (see the discussion section) and has been added *a posteriori* to the simulation results. The model instead overestimates the release of Na and Si, suggesting that plants and fungi in the experiments might have driven incongruent dissolution reactions. It might also be that the Si experimental values are biased low due to underestimation of the Si pool by extraction with ammonium acetate (Wang et al., 2004). There is also a promising model-experiment agreement in the Ca, Mg, and Si partitioning among soil, plant, and leachate (Figure S7 in Supporting Information S1). Moreover, the model effectively reproduces the potential CO₂ sequestration resulting from alkaline element release, demonstrating substantially higher values in both experiments and simulations than the effective CO₂ sequestered through

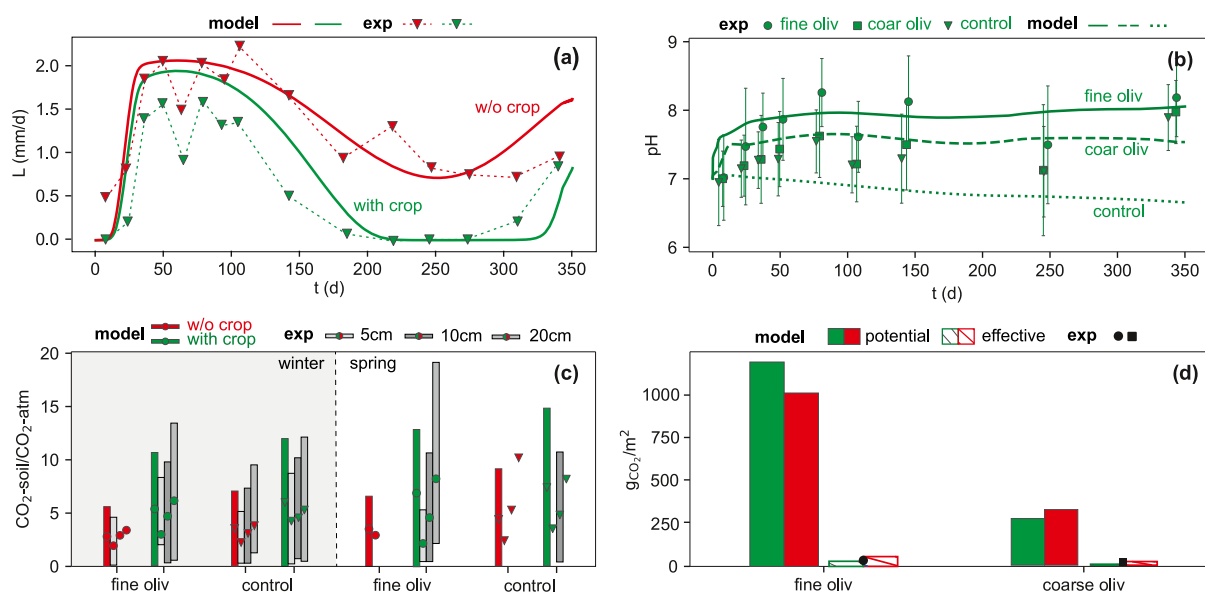


Figure 6. Model-experiment comparison based on the mesocosm experiments by Amann et al. (2020) in the presence (green) and absence (red) of vegetation. (a) Leaching fluxes. Experimental leaching fluxes are from the control experiments. (b) pH dynamics in the presence of vegetation. The reported experimental values are averages between shallow (1.5 cm) and deep (24 cm) measurements. Error bars on experimental values indicate ± 1 SD. Figure S8 in Supporting Information S1 shows the equivalent plot in the absence of vegetation. (c) Soil air CO_2 , showing experimental measurements obtained at different depths compared with depth-averaged model results. Bars indicate ± 1 SD associated with time variability (model) and experimental replicates when available. For the numerical results, winter and spring are defined as the experiment's first and second 100 days, respectively. (d) Potential and effective CO_2 sequestration, with experimental results showcasing averaged effective CO_2 sequestration with and without vegetation.

aqueous carbonate leaching. The difference is primarily due to CEC adsorption, with plant uptake playing a minor role (Figure S7 in Supporting Information S1).

3.3.2. Rain Barrels

Amann et al. (2020) performed experiments in rain barrels measuring 46 cm in diameter and 26 cm in depth over a year. The soil was classified as loamy sand with an initial pH of 7 and an initial OC content of 1.2%. The simulations mimic a rainfall regime of 800 mm/yr, with rainfall events distributed every day or week, with little difference in the results between the two cases. The particle size distributions differentiate between coarse and fine olivine (mostly forsterite, Mg_2SiO_4) applications of 22 kg/m², with 25 and 720 μm being the dominant diameter classes, respectively. The simulations assume that the olivine is mixed across the barrel, while, in the experiments, olivine was mixed in the top layer of approximately 11 cm. Temperature was varied with a sinusoidal function across the year, from a minimum of 6°C to a maximum of 25°C. The CEC was fixed at the experimental value of 8.6 cmol_c/kg_{soil}, initially saturated by 86.5% of Ca, 5% of Mg, 5% of K, 3% of Na, and 0.5% of H and Al (Amann et al., 2020). We ran six simulations for the control case and the coarse and fine olivine applications, with and without vegetation.

Figure 6 presents the model-experiment comparisons in terms of hydrological balance (a), pH dynamics (b), soil air CO_2 (c), and CO_2 sequestration (d). For this experimental setup, leaching is a significant proxy for hydrologic partitioning since evapotranspiration directly results from the difference between water input and leaching. The simulations reproduce the leaching seasonal patterns due to the impact of temperature and vegetation. However, the experiments revealed a slightly different water partitioning due to rock application altering the soil hydraulic property, which the model cannot reproduce (Amann et al., 2020). The soil bulk pH dynamics show reasonable agreement in the barrels with rock powder applications, with an increase over time due to olivine dissolution. Model results and observations do not match for the control barrels, where the experimental pH shows a considerable increase in soil pH even in the absence of rock powder. Both simulation and experiments show how vegetation tends to reduce the pH by cation uptake and CO_2 respiration (Figure 6b and Figure S8 in Supporting Information S1). The soil air CO_2 dynamics also show promising results, with the model reproducing seasonal variations and the influence of the vegetation in increasing the CO_2 concentration (Figure 6c).

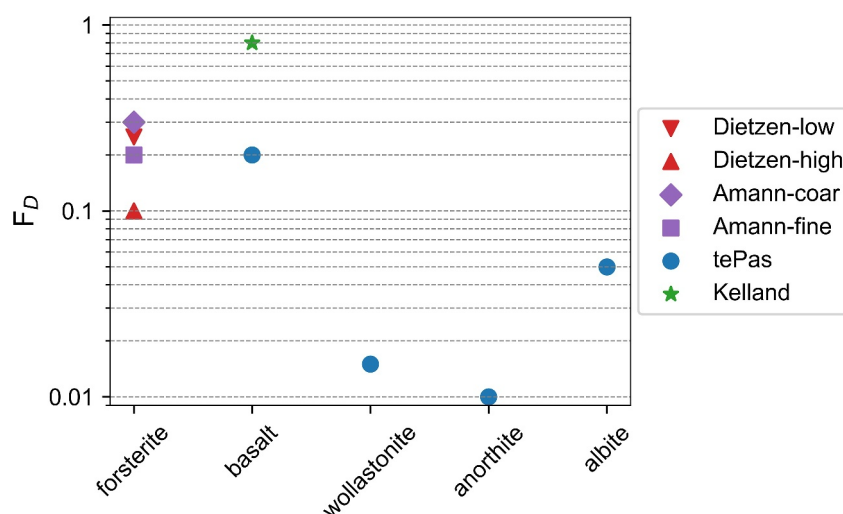


Figure 7. Dissolution factor (F_D) used in the weathering rate Equation 10 to reproduce the experimental observations of alkalinity releases.

Regarding CO_2 sequestration, we estimated the potential CO_2 capture due to the Mg released by mineral dissolution and the effective CO_2 capture, here quantified through the Mg observed in the leached water, as done in the experimental work. Note that the experimental effective CO_2 capture has been reassessed from Mg leachate data due to a dimensional inconsistency in Formula 2 reported by Amann et al. (2020). The potential CO_2 capture is much higher than the effective one due to the loss of alkaline cations to soil adsorption and plant uptake. Interestingly, vegetation has a dual influence on CO_2 removal: plant uptake of alkaline cations reduces the effective CO_2 removal, but plant-induced soil acidification enhances the mineral dissolution rates, increasing the potential CO_2 removal. Consequently, our results suggest a trade-off in CO_2 removal efficiency, with plant-absent scenarios showcasing slower but more efficient removal processes. In contrast, plant-present scenarios feature faster but less efficient removal processes.

4. Discussion

The overall favorable agreement between model outcomes and experimental observations allows us to provide critical insights into the weathering rates. We then identify and discuss areas requiring further theoretical and experimental exploration.

4.1. Weathering Rates

The assessment of EW is intricately linked to the precise determination of rock weathering rates, whose parameters are surrounded by considerable uncertainty (Calabrese et al., 2022). The theoretical formulation used here (Palandri, 2004) is widely regarded as comprehensive and is commonly applied in EW assessments (Beerling et al., 2020; Kantzas et al., 2022; Kanzaki et al., 2022; Taylor et al., 2016). However, this formulation is derived from experimental data from stirred reactors without diffusive limitations and under conditions far from equilibrium. In the complex, multiphase, and porous soil environment, numerous overlooked biotic and abiotic processes may influence dissolution rates: (a) concentration gradient formation into the aqueous phase near mineral surfaces, (b) primary and secondary mineral coatings, (c) fungal and bacterial activity, (d) catalyzation or inhibition of the dissolution reactions due to the presence of other chemical species. While some specific processes are expected to promote dissolution (e.g., biotic activity), others predominantly impede it (e.g., particle coatings). As a result, the validity of the formula for EW applications remains an open question.

Our model-experiment comparison indicates that Palandri's formulation requires, at a minimum, a correction factor for dissolution, F_D in (10), which is consistently below one for most experimental setups and rock types (Figure 7). This discrepancy underscores a substantial gap between theoretical and observed dissolution rates, likely due to the complex abiotic and biotic environmental factors that standard weathering rate definitions fail to capture. These findings may not be unexpected: similar discrepancies have frequently been reported in soil rock

weathering beyond the context of EW (Brantley, 2003; Jung & Navarre-Sitchler, 2018; Schabernack & Fischer, 2022), as well as in organic matter decomposition (Davidson & Janssens, 2006), and they align with Palandri's observation that *actual equilibration rates are expected to be much slower than those predicted by the selected computer code* (Palandri, 2004). Additionally, while the precise estimate of F_D for each specific model-data comparison involves various uncertainties in process representations and parameter values, these uncertainties are overshadowed by the much more significant uncertainty in weathering rates, which spans several orders of magnitude and exerts the most critical control over the entire EW dynamics.

The discrepancy between theoretical expectations and observations carries significant implications. Weathering rates are the main control of the carbon sequestration process. Unless field weathering rates are substantially higher than those observed in small-scale experiments, our results suggest that previous model-based EW assessments - considering $F_D \geq 1$ due to biotic processes (Beerling et al., 2020; Kantzas et al., 2022) - may overestimate the potential of EW for CO₂ removal by orders of magnitude. To accurately assess the feasibility and effectiveness of EW in climate mitigation, narrowing down uncertainties in weathering rates will be essential. Both model advances and extensive data collection will be required to gain mechanistic insights into F_D and shift models like SMEW from needing an observation-based calibration of weathering rates to models with inherent predictive capabilities. Emergent field and laboratory data collection will be critical in constraining the relationships between weathering rates and specific mineral types, soil and crop characteristics, and climates. Model improvements will need to systematically incorporate the above-mentioned soil biotic and abiotic processes that can influence weathering rates, including microbial activity and mineral surface reactivity (Schabernack & Fischer, 2022).

4.2. Limitations and Outlook

The model-experiment comparison presented in this study is only a first step toward having robust assessments of EW models to reproduce observations across scales. Many advances will be needed from both modeling and observational perspectives.

From a modeling point of view, the model presented here accounts for the primary variables of interest to assess the fate of the alkaline cations released by the EW applications and their corresponding inorganic carbon sequestration potential. In addition to model advances needed to gain mechanistic insights into weathering rates, extensions could include feedback that the rock powder application may have on some soil physical and biotic processes. The different leaching fluxes observed in the experiments by Amann et al. (2020) suggest that the rock powder impacts the soil texture and hydraulic conductivity, hence the soil water partitioning. Specific experiments evaluating the temporal evolution of soil physical properties are needed to incorporate such feedback in models, even though some theoretical estimates may be derived based on soil physics models (Jury & Horton, 2004). Furthermore, rock applications may influence biotic activity and the OC balance, with potentially detrimental effects in tropical soils and peatlands (Klemme et al., 2022). Modeling advances could also include mass balances for heavy metal accumulations, such as nickel and copper, which are significant concerns in the context of EW applications (Dupla et al., 2023; Haque et al., 2020).

Compared to more popular reactive transport models, SMEW is more parsimonious, not accounting for soil vertical heterogeneity and including fewer chemical species. This simplicity comes at the cost of spatial information but at the advantage of accessibility and a more focused examination of temporal dynamics. Interestingly, our model does not necessitate a semi-empirical pH buffer function often employed in EW simulations with reactive transport models to avoid unrealistic spikes in soil pH. This is intriguing since our buffering mechanisms incorporate only carbonate chemistry and cation adsorption while neglecting others like organic alkalinity. On the contrary, our model encounters limitations in reproducing the rapid dissolution of certain minerals and materials (e.g., Ca(OH)₂) due to pronounced spikes in alkalinity that hinder the numerical convergence of the implicit system (Appendix A). Looking ahead, a promising avenue involves integrating our model results with both reactive transport models and observational data to gain comprehensive insights into soil EW dynamics.

From an experimental standpoint, it is worth acknowledging the temporal constraint within the available data sets (Table S1). Specifically, only one of the experimental data sets used within this study spans a complete year (Amann et al., 2020), while others have a relatively shorter duration of a few months. Given the potential yearly timescales associated with the dissolution of EW rock powder, extrapolating results becomes challenging, especially considering that weathering rates may decrease over the years (Figure S1 in Supporting

Information S1). Additionally, most experiments relied on elevated rock loadings (i.e., $\geq 10 \text{ kg/m}^2$) to enhance signals within the short experimental time frame, although such loadings may not be realistic for practical applications. There is also an opportunity to explore the influence of realistic stochastic rainfall regimes, often absent in current experimental setups.

Integrating field observations of large-scale EW applications will hopefully address some of these temporal and loading limitations, offering insights into the alignment between model results, small-scale experiments, and the practical considerations of large-scale field trials. Optimizing the spatial and temporal frequency of data collection will be crucial to planning feasible field campaigns while preserving quantitative information on soil heterogeneity and temporal dynamics caused by seasonal and daily fluctuations in hydrological and biogeochemical quantities. Priority should be given to measuring the partitioning of released alkaline cations among leaching fluxes, plant uptake, and soil adsorption. This serves a dual purpose: (a) quantifying weathering rates and (b) understanding the discrepancy between effective and potential CO_2 sequestration. Additionally, since the movement of alkaline cations extends into deeper soil layers and stream networks, conducting coupled measurements within connected streams can help quantify the actual travel time and flux of the weathering products. Lastly, although SMEW is parsimonious with respect to the complexity of hydrological and biogeochemical processes in soils, it still consists of multiple state variables, parameters, and highly nonlinear interactions. With the increasing availability of data from laboratory and field experiments, Bayesian approaches with information criteria metrics can be a valuable approach to solving inverse problems, simultaneously estimating parameters and their uncertainty while also accounting for model complexity.

5. Conclusions

While EW holds great promise as a negative emission strategy, thanks to its significant CDR potential, low technological prerequisites, and valuable co-benefits, no model has been shown to reproduce EW observations at scale. This deficit restricts our ability to make accurate quantitative predictions for assessments of CDR via EW. In this study, we took a benchmark step in this direction, developing a relatively accessible ecohydrological and biogeochemical model whose results could be meticulously compared with four distinct experimental data sets of different complexity.

The model-experiment comparison demonstrates an overall favorable agreement for the primary variables of interest, including water partitioning, alkalinity release, pH dynamics, and CO_2 sequestration. The comparison also demonstrates that weathering rates are lower than traditionally assumed by one or two orders of magnitudes and highlights further research directions to improve our understanding and quantitative predictive power for EW as a NET. Finally, while representing EW dynamics within the soil's upper layers is crucial, EW negative emission potential is linked to the fate of rock dissolution products from the field to the ocean (Bertagni et al., 2024; Calabrese et al., 2022; Hartmann et al., 2013), a journey yet to be fully disclosed.

Appendix A: Implicit System of Equilibrium Equations

We here report the implicit system of equilibrium equations solved under the quasi-steady approximation jointly with the system of ODEs (1)–(8). These equations are all coupled and quantify how total quantities within the soil control volume of depth Z are distributed among the different soil phases. Specifically, alkaline cations (X_{tot}) are distributed between dissolved and adsorbed phases, inorganic carbon (IC_{tot}) is distributed between aqueous and air phases, and aluminum (Al_{tot}) exists dissolved in water, adsorbed to the soil matrix or in complexes with organic or inorganic matter. In formula

$$X_{\text{tot}} = n_Z s[X] + f_X \text{CEC} / n_X, \quad (\text{A1})$$

$$\text{IC}_{\text{tot}} = n_Z s[\text{DIC}] + n_Z (1 - s)[\text{CO}_2]_a, \quad (\text{A2})$$

$$\text{Al}_{\text{tot}} = n_Z s[\text{Al}]_{\text{mob}} + f_{\text{Al}} \text{CEC} / 3 + \text{Al}_{\text{imm}}, \quad (\text{A3})$$

where n_X is the cation valence and CEC is the CEC. The latter indicates the moles of dissolved cations that can be adsorbed on soil colloids due to their negatively charged surface (Weil & Brady, 2016).

Cation Partitioning and Soil Adsorption. The master variable connecting alkaline cations and carbonate system is alkalinity (Alk). Expressed in terms of species that are conservative to changes in pH, temperature, and pressure (Bertagni & Porporato, 2022; Wolf-Gladrow et al., 2007), alkalinity is

$$[\text{Alk}] = 2[\text{Ca}^{2+}] + 2[\text{Mg}^{2+}] + [\text{K}^{2+}] + [\text{Na}^{2+}] - [\text{An}], \quad (\text{A4})$$

where [An] indicates the cumulative concentration of the anions of the strong acids. Quantifying the dissolved cations in the soil solution requires assessing the cation partitioning between the dissolved and adsorbed phases. This is done using the Gaines-Thomas convention (Bleam, 2017). Specifically, five equations are used to describe the binary exchange of Ca^{2+} with Al^{3+} , Mg^{2+} , Na^+ , K^+ , and H^+ :

$$\frac{f_{\text{Ca}}^3}{f_{\text{Al}}^2} = K_{\text{Ca-Al}} \frac{[\text{Ca}^{2+}]^3}{[\text{Al}^{3+}]^2}, \quad \frac{f_{\text{Ca}}}{f_{\text{Mg}}} = K_{\text{Ca-Mg}} \frac{[\text{Ca}^{2+}]}{[\text{Mg}^{2+}]}, \quad \frac{f_{\text{Ca}}}{f_{\text{K}}^2} = K_{\text{Ca-K}} \frac{[\text{Ca}^{2+}]}{[\text{K}^+]^2}, \quad (\text{A5})$$

where the exchange equations for Ca-Na and Ca-H are equivalent to Ca-K. The soil-dependent cation exchange constants can be evaluated with coupled measurements of adsorbed and dissolved species or can be evaluated after the extensive data set of Vries and Posch (2003). The sum of all exchangeable fractions (f) is equal to unity, namely

$$f_{\text{Ca}} + f_{\text{Al}} + f_{\text{Mg}} + f_{\text{Na}} + f_{\text{K}} + f_{\text{H}} = 1. \quad (\text{A6})$$

Air-Water Carbonate System. In the soil solutions, and more generally in natural waters, the alkalinity charge difference expressed in A4 is balanced by the aqueous carbonate system.

$$[\text{Alk}] = [\text{HCO}_3^-] + 2[\text{CO}_3^{2-}] + [\text{OH}^-] - [\text{H}^+], \quad (\text{A7})$$

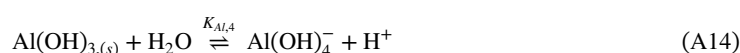
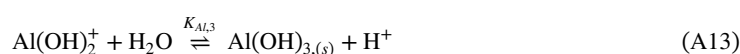
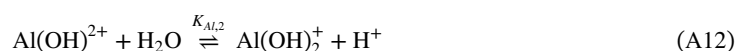
$$[\text{DIC}] = [\text{CO}_2]_w + [\text{HCO}_3^-] + [\text{CO}_3^{2-}] \quad (\text{A8})$$

$$[\text{HCO}_3^-] = K_1[\text{CO}_2]_w/[\text{H}^+], \quad [\text{CO}_3^{2-}] = K_1K_2[\text{CO}_2]_w/[\text{H}^+]^2, \quad (\text{A9})$$

$$[\text{CO}_2]_a = K_{\text{H}}[\text{CO}_2]_w, \quad [\text{OH}^-] = [\text{H}^+]/K_w, \quad (\text{A10})$$

where K_1 and K_2 are the first and second carbonic acid dissociation constants. K_w is the water dissociation constant. K_{H} is Henry's constant for CO_2 solubility. All these constants and their temperature dependence are evaluated after Stumm and Morgan (1996). The combination of Equations A4 and A7 summarizes EW's goal of increasing alkalinity by mineral dissolution to promote aqueous carbonate formation. The efficiency of this process varies as a function of the water chemistry (Bertagni & Porporato, 2022). Formal extensions to the alkalinity definition A7 could include aluminum, which plays a buffer role in acidic conditions, and organic alkalinity. Other weak acids and bases have been shown to play a negligible role in the soil solution (Bertagni & Porporato, 2022).

Aluminum Speciation. Aluminum chemistry is complex and strongly influenced by water pH (Nordstrom & May, 2020; Weil & Brady, 2016). Aluminum in aqueous systems speciates into five main monomeric species, following the reactions



where the constants K_{Al} are evaluated after Weil and Brady (2016). In highly acidic ($pH < 4.5$) and highly alkaline ($pH > 7$) conditions, aluminum solubility is enhanced, and the dominant species are dissolved Al^{3+} and $Al(OH)_4^-$, respectively. By contrast, at intermediate pH values ($5 < pH < 7$), Al is present in less mobile forms, such as the hydroxy aluminum ions $Al(OH)^{2+}$ and $Al(OH)_2^+$, which typically form complexes with organic matter and other soil elements, as well as the solid mineral gibbsite $Al(OH)_3$. We hence discriminate into mobile ($[Al]_{mob}$) and immobile (Al_{imm}) aluminum pools following

$$[Al]_{mob} = [Al^{3+}] + [Al(OH)_4^-], \quad (A15)$$

$$Al_{imm} = ([Al(OH)^{2+}] + [Al(OH)_2^+] + [Al(OH)_3]) nZs. \quad (A16)$$

We then consider that only the mobile Al can be lost through leaching events; see Equation 8.

Appendix B: Plant Dynamics and Their Role in EW

In SMEW, plants influence EW dynamics by impacting soil hydrological and biogeochemical balances. Plant roots transpire water, actively and passively uptake nutrients, and release inorganic carbon (autotrophic respiration). Growing vegetation (V) can be dynamically modeled through a classical logistic equation

$$\frac{dV}{dt} = \alpha_V V (k_V - V), \quad (B1)$$

where k_V is the carrying capacity per unit area, dependent on plant and ecosystem types, and α_V is the plant growth rate. The growth rate can be estimated based on the time (t_V) required for plants to progress from seedling to maturity through $\alpha_V \approx 6/t_V$. Simulated plant-mediated processes are then scaled with the normalized vegetation variable $\hat{V} = V/k_V$, defined between 0 and 1. These processes include: (a) plant transpiration (T), modeled as a soil moisture function (Laio et al., 2001); (b) plant passive uptake, assumed to be directly proportional to the transpiration rate (Cipolla et al., 2021a); (c) autotrophic respiration ($RESP_a$), estimated to be equivalent to heterotrophic respiration when plants are fully grown (Bond-Lamberty et al., 2004); (d) active uptake, which occurs during plant growth when passive uptake alone cannot meet the nutrient demands for growth (see below). Noteworthy, both plant-mediated nutrient uptake and inorganic carbon release processes contribute to soil acidification.

In addition to the nutrient uptake through the transpiration stream (passive uptake), plants can also rely on more complex and energetically expensive physiological processes (active uptake) when the passive uptake is insufficient to meet the nutrient demand (DEM). The active uptake then counts on a diffusion flux from the bulk of the solution to the plant roots (Grathwohl, 1998; Porporato, D'Odorico, et al., 2003; Porporato & Yin, 2022). Here we propose a new modeling framework for the plant active uptake wherein the diffusive flux is quantified by the root surface area (i.e., the root area index, RAI), the element diffusivity in water (D_w), and the concentration gradient between the root surface and the solution bulk. Assuming a null element concentration on the root surface and taking calcium (Ca) as an example, the concentration gradient is $[Ca]/\ell$, where ℓ is the typical distance traveled from bulk to root. The latter can be quantified as $\ell = \sqrt{d_r Z / (\hat{V} \cdot RAI)}$, assuming parallel cylindrical roots of average diameter d_r uniformly distributed over the depth Z (Manzoni et al., 2013) and considering that the root surface area scales with the vegetation stage. Active uptake for Ca can then be expressed as

$$UP_{Ca} = \begin{cases} 0 & \text{if } [Ca]T \geq DEM_{Ca} \\ \min\left(\hat{V} \cdot RAI \cdot D_w \frac{[Ca]}{\ell}, DEM_{Ca} - T[Ca]\right) & \text{if } [Ca]T < DEM_{Ca} \end{cases} \quad (B2)$$

DEM_{Ca} defines the calcium required for the plant's new biomass development ($DEM_{Ca} = \xi_{Ca} dV/dt$), with ξ_{Ca} being a plant-dependent coefficient specifying moles of Ca per biomass unit. Similar equations apply to other essential plant nutrients, including Mg, K, and Si.

Data Availability Statement

The numerical codes for SMEW (Python), the Jupyter Notebooks for the model-experiment comparisons, and all numerical data produced within this manuscript are available on GitHub (<https://github.com/MatteoBertagni/SMEW>) and on Zenodo (Bertagni, 2024). The experimental data come from previous works, as acknowledged in the manuscript.

Acknowledgments

L.V.N. acknowledges support by European Union NextGenerationEU – National Recovery and Resilience Plan (PNRR), Mission 4, Component 2, PRIN 2022 PNRR P20225K9YW – CUP B53D23033470001. We thank M. Kelland and E. tePas for helpful discussions regarding the experimental results. M.B.B. acknowledges S.K. Anand for the suggestions on the numerical coding. M.B.B. and A.P. were supported by the BP through the Carbon Mitigation Initiative at Princeton University.

References

- Allen, R. G., Pereira, L. S., Raes, D., & Smith, M. (Eds.). (1998). *Crop evapotranspiration: Guidelines for computing crop water requirements* (No. 56). Food and Agriculture Organization of the United Nations.
- Amann, T., & Hartmann, J. (2022). Carbon accounting for enhanced weathering. *Frontiers in Climate*, 4. <https://doi.org/10.3389/fclim.2022.849948>
- Amann, T., Hartmann, J., Struyf, E., de Oliveira Garcia, W., Fischer, E. K., Janssens, I., et al. (2020). Enhanced weathering and related element fluxes – A cropland mesocosm approach. *Biogeosciences*, 17(1), 103–119. <https://doi.org/10.5194/bg-17-103-2020>
- Baek, S. H., Kanzaki, Y., Lora, J. M., Planavsky, N., Reinhard, C. T., & Zhang, S. (2023). Impact of climate on the global capacity for enhanced rock weathering on croplands. *Earth's Future*, 11(8), e2023EF003698. <https://doi.org/10.1029/2023EF003698>
- Beerling, D. J., Kantzas, E. P., Lomas, M. R., Wade, P., Eufrazio, R. M., Renforth, P., et al. (2020). Potential for large-scale CO₂ removal via enhanced rock weathering with croplands. *Nature*, 583(7815), 242–248. <https://doi.org/10.1038/s41586-020-2448-9>
- Berge, H. F. M. t., Meer, H. G. v. d., Steenhuizen, J. W., Goedhart, P. W., Knops, P., & Verhagen, J. (2012). Olivine weathering in soil, and its effects on growth and nutrient uptake in Ryegrass (*Lolium perenne* L.): A pot experiment. *PLoS One*, 7(8), e42098. <https://doi.org/10.1371/journal.pone.0042098>
- Bertagni, M. B. (2024). SMEW [Software]. Zenodo. <https://doi.org/10.5281/zenodo.14356661>
- Bertagni, M. B., & Porporato, A. (2022). The carbon-capture efficiency of natural water alkalization: Implications for enhanced weathering. *Science of the Total Environment*, 838, 156524. <https://doi.org/10.1016/j.scitotenv.2022.156524>
- Bertagni, M. B., Regnier, P., Yan, Y., & Porporato, A. (2024). A dimensionless framework for the partitioning of fluvial inorganic carbon. *Geophysical Research Letters*, 51(19), e2024GL111310. <https://doi.org/10.1029/2024GL111310>
- Blanc-Betes, E., Kantola, I. B., Gomez-Casanovas, N., Hartman, M. D., Parton, W. J., Lewis, A. L., et al. (2021). In silico assessment of the potential of basalt amendments to reduce N₂O emissions from bioenergy crops. *GCB Bioenergy*, 13(1), 224–241. <https://doi.org/10.1111/gcbb.12757>
- Bleam, W. F. (2017). *Soil and environmental chemistry* (2nd ed.). Elsevier/AP, Academic Press is an imprint of Elsevier.
- Bond-Lamberty, B., Wang, C., & Gower, S. T. (2004). A global relationship between the heterotrophic and autotrophic components of soil respiration? *Global Change Biology*, 10(10), 1756–1766. <https://doi.org/10.1111/j.1365-2486.2004.00816.x>
- Brantley, S. L. (2003). Reaction kinetics of primary rock-forming minerals under ambient conditions. In *Surface and ground water, weathering, and soils* (Vols. 5–9, pp. 73–117). Elsevier Inc. <https://doi.org/10.1016/B0-08-043751-6/05075-1>
- Buckingham, F. L., Henderson, G. M., Holdship, P., & Renforth, P. (2022). Soil core study indicates limited CO₂ removal by enhanced weathering in dry croplands in the UK. *Applied Geochemistry*, 147, 105482. <https://doi.org/10.1016/j.apgeochem.2022.105482>
- Calabrese, S., & Porporato, A. (2020). Wetness controls on global chemical weathering. *Environmental Research Communications*, 2(8), 085005. <https://doi.org/10.1088/2515-7620/abad7b>
- Calabrese, S., Wild, B., Bertagni, M. B., Bourg, I. C., White, C., Aburto, F., et al. (2022). Nano-to global-scale uncertainties in terrestrial enhanced weathering. *Environmental Science & Technology*, 56(22), 15261–15272. (Publisher: American Chemical Society). <https://doi.org/10.1021/acs.est.2c03163>
- Calvin, K., Dasgupta, D., Krinner, G., Mukherji, A., Thorne, P. W., Trisos, C., et al. (2023). IPCC, 2023: Climate change 2023: Synthesis report. Contribution of working Groups I, II and III to the sixth assessment report of the intergovernmental panel on climate change. In Core Writing Team, H. Lee, & J. Romero (Eds.), *IPCC, Geneva, Switzerland. (Tech. Rep.)*. Intergovernmental Panel on Climate Change (IPCC). <https://doi.org/10.59327/IPCC/AR6-9789291691647>
- Cipolla, G., Calabrese, S., Noto, L. V., & Porporato, A. (2021a). The role of hydrology on enhanced weathering for carbon sequestration II. From hydroclimatic scenarios to carbon-sequestration efficiencies. *Advances in Water Resources*, 154, 103949. <https://doi.org/10.1016/j.advwatres.2021.103949>
- Cipolla, G., Calabrese, S., Noto, L. V., & Porporato, A. (2021b). The role of hydrology on enhanced weathering for carbon sequestration I. Modeling rock-dissolution reactions coupled to plant, soil moisture, and carbon dynamics. *Advances in Water Resources*, 154, 103934. <https://doi.org/10.1016/j.advwatres.2021.103934>
- Clarkson, M. O., Larkin, C., Swoboda, P., Reershemius, T., Suhrhoff, J. T., Maesano, C. N., & Campbell, J. (2023). A review of measurement for quantification of carbon dioxide removal by enhanced weathering in soil. Retrieved from <https://eartharxiv.org/repository/view/6317/> (Publisher: EarthArXiv)
- Davidson, E. A., & Janssens, I. A. (2006). Temperature sensitivity of soil carbon decomposition and feedbacks to climate change. *Nature*, 440(7081), 165–173. <https://doi.org/10.1038/nature04514>
- Deng, K., Yang, S., & Guo, Y. (2022). A global temperature control of silicate weathering intensity. *Nature Communications*, 13(1), 1781. Number: 1 Publisher: Nature Publishing Group. <https://doi.org/10.1038/s41467-022-29415-0>
- Dietzen, C., Harrison, R., & Michelsen-Correa, S. (2018). Effectiveness of enhanced mineral weathering as a carbon sequestration tool and alternative to agricultural lime: An incubation experiment. *International Journal of Greenhouse Gas Control*, 74, 251–258. <https://doi.org/10.1016/j.ijggc.2018.05.007>
- Dietzen, C., & Rosing, M. T. (2023). Quantification of CO₂ uptake by enhanced weathering of silicate minerals applied to acidic soils. *International Journal of Greenhouse Gas Control*, 125, 103872. <https://doi.org/10.1016/j.ijggc.2023.103872>
- Dong, X., Richter, D. D., Thompson, A., & Wang, J. (2023). The primacy of temporal dynamics in driving spatial self-organization of soil iron redox patterns. *Proceedings of the National Academy of Sciences*, 120(51), e2313487120. <https://doi.org/10.1073/pnas.2313487120>
- Dupla, X., Möller, B., Baveye, P. C., & Grand, S. (2023). Potential accumulation of toxic trace elements in soils during enhanced rock weathering. *European Journal of Soil Science*, 74(1), e13343. <https://doi.org/10.1111/ejss.13343>
- Fauteux, F., Rémus-Borel, W., Menzies, J. G., & Bélanger, R. R. (2005). Silicon and plant disease resistance against pathogenic fungi. *FEMS Microbiology Letters*, 249(1), 1–6. <https://doi.org/10.1016/j.femsle.2005.06.034>

- Grathwohl, P. (1998). *Diffusion in natural porous media: Contaminant transport, sorption/desorption and dissolution kinetics*. Springer US. (OCLC: 851794035).
- Hamilton, S. K., Kurzman, A. L., Arango, C., Jin, L., & Robertson, G. P. (2007). Evidence for carbon sequestration by agricultural liming: Fate of carbon in agricultural lime. *Global Biogeochemical Cycles*, 21(2). <https://doi.org/10.1029/2006GB002738>
- Haque, F., Chiang, Y. W., & Santos, R. M. (2020). Risk assessment of Ni, Cr, and Si release from alkaline minerals during enhanced weathering. *Open Agriculture*, 5(1), 166–175. <https://doi.org/10.1515/opag-2020-0016>
- Hartmann, J., West, A. J., Renforth, P., Köhler, P., De La Rocha, C. L., Wolf-Gladrow, D. A., et al. (2013). Enhanced chemical weathering as a geoengineering strategy to reduce atmospheric carbon dioxide, supply nutrients, and mitigate ocean acidification: Enhanced weathering. *Reviews of Geophysics*, 51(2), 113–149. <https://doi.org/10.1002/rog.20004>
- Jha, A., Bonetti, S., Smith, A. P., Souza, R., & Calabrese, S. (2023). Linking soil structure, hydraulic properties, and organic carbon dynamics: A holistic framework to study the impact of climate change and land management. *Journal of Geophysical Research: Biogeosciences*, 128(7), e2023JG007389. <https://doi.org/10.1029/2023JG007389>
- Jung, H., & Navarre-Sitchler, A. (2018). Physical heterogeneity control on effective mineral dissolution rates. *Geochimica et Cosmochimica Acta*, 227, 246–263. <https://doi.org/10.1016/j.gca.2018.02.028>
- Jury, W. A., & Horton, R. (2004). *Soil physics*. John Wiley & Sons. (Google-Books-ID: E5HZDwAAQBAJ).
- Kantzas, E. P., Val Martin, M., Lomas, M. R., Eufrazio, R. M., Renforth, P., Lewis, A. L., et al. (2022). Substantial carbon drawdown potential from enhanced rock weathering in the United Kingdom. *Nature Geoscience*, 1–8(5), 382–389. <https://doi.org/10.1038/s41561-022-00925-2>
- Kanzaki, Y., Zhang, S., Planavsky, N. J., & Reinhard, C. T. (2022). Soil cycles of elements simulator for predicting TERrestrial regulation of greenhouse gases: SCEPTER v0.9. *Geoscientific Model Development*, 15(12), 4959–4990. <https://doi.org/10.5194/gmd-15-4959-2022>
- Kelland, M. E., Wade, P. W., Lewis, A. L., Taylor, L. L., Sarkar, B., Andrews, M. G., et al. (2020). Increased yield and CO₂ sequestration potential with the C4cereal-Sorghum bicolor-cultivated in basaltic rock dust-amended agricultural soil. *Global Change Biology*, 26(6), 3658–3676. <https://doi.org/10.1111/gcb.15089>
- Kim, Y.-H., Khan, A. L., Kim, D.-H., Lee, S.-Y., Kim, K.-M., Waqas, M., et al. (2014). Silicon mitigates heavy metal stress by regulating P-type heavy metal ATPases, Oryza sativalow silicon genes, and endogenous phytohormones. *BMC Plant Biology*, 14(1), 13. <https://doi.org/10.1186/1471-2229-14-13>
- Kirk, G. J. D., Versteegen, A., Ritz, K., & Milodowski, A. E. (2015). A simple reactive-transport model of calcite precipitation in soils and other porous media. *Geochimica et Cosmochimica Acta*, 165, 108–122. <https://doi.org/10.1016/j.gca.2015.05.017>
- Klemme, A., Rixen, T., Müller, M., Notholt, J., & Warneke, T. (2022). Destabilization of carbon in tropical peatlands by enhanced weathering. *Communications Earth & Environment*, 3(1), 1–9. Number: 1 Publisher: Nature Publishing Group. <https://doi.org/10.1038/s43247-022-00544-0>
- Knapp, W. J., Stevenson, E. I., Renforth, P., Ascough, P. L., Knight, A. C. G., Bridgestock, L., et al. (2023). Quantifying CO₂ removal at enhanced weathering sites: A multiproxy approach. *Environmental Science & Technology*, 57(26), 9854–9864. <https://doi.org/10.1021/acs.est.3c03757>
- Köhler, P., Hartmann, J., & Wolf-Gladrow, D. A. (2010). Geoengineering potential of artificially enhanced silicate weathering of olivine. *Proceedings of the National Academy of Sciences of the United States of America*, 107(47), 20228–20233. <https://doi.org/10.1073/pnas.1000545107>
- Laio, F., Porporato, A., Ridolfi, L., & Rodriguez-Iturbe, I. (2001). Plants in water-controlled ecosystems: Active role in hydrologic processes and response to water stress II. Probabilistic soil moisture dynamics. *Advances in Water Resources*, 17.
- Larkin, C. S., Andrews, M. G., Pearce, C. R., Yeong, K. L., Beerling, D. J., Bellamy, J., et al. (2022). Quantification of CO₂ removal in a large-scale enhanced weathering field trial on an oil palm plantation in Sabah, Malaysia. *Frontiers in Climate*, 4. <https://doi.org/10.3389/fclim.2022.959229>
- Lasaga, A. C. (1984). Chemical kinetics of water-rock interactions. *Journal of Geophysical Research*, 89(B6), 4009–4025. <https://doi.org/10.1029/JB089iB06p04009>
- Li, P., Deng, H., & Molins, S. (2022). The effect of pore-scale two-phase flow on mineral reaction rates. *Frontiers in Water*, 3. <https://doi.org/10.3389/frwa.2021.734518>
- Maher, K., Steefel, C. I., White, A. F., & Stonestrom, D. A. (2009). The role of reaction affinity and secondary minerals in regulating chemical weathering rates at the Santa Cruz Soil Chronosequence, California. *Geochimica et Cosmochimica Acta*, 73(10), 2804–2831. <https://doi.org/10.1016/j.gca.2009.01.030>
- Manzoni, S., Schimel, J. P., & Porporato, A. (2012). Responses of soil microbial communities to water stress: Results from a meta-analysis. *Ecology*, 93(4), 930–938. <https://doi.org/10.1890/11-0026.1>
- Manzoni, S., Vico, G., Porporato, A., & Katul, G. (2013). Biological constraints on water transport in the soil–plant–atmosphere system. *Advances in Water Resources*, 51, 292–304. <https://doi.org/10.1016/j.advwatres.2012.03.016>
- Miele, F., Benettin, P., Wang, S., Retti, I., Asadollahi, M., Fruttschi, M., et al. (2023). Spatially explicit linkages between redox potential cycles and soil moisture fluctuations. *Water Resources Research*, 59(3), e2022WR032328. <https://doi.org/10.1029/2022WR032328>
- Millington, R. J., & Quirk, J. P. (1961). Permeability of porous solids. *Transactions of the Faraday Society*, 57, 1200. <https://doi.org/10.1039/tf9615701200>
- Morel, F., & Hering, J. G. (1993). *Principles and applications of aquatic chemistry*. Wiley.
- Nordstrom, D. K., & May, H. M. (2020). Aqueous equilibrium data for mononuclear aluminum species. In G. Sposito (Ed.), *The environmental chemistry of aluminum* (2nd ed., pp. 39–80). CRC Press. <https://doi.org/10.1201/9780138736781-2>
- Palandri, K. (2004). *Rate parameters of water-mineral interaction kinetics for application to geochemical modeling*. (Open-File Report) (Series: Open-File Report). USGS.
- Porporato, A., D'Odorico, P., Laio, F., & Rodriguez-Iturbe, I. (2003). Hydrologic controls on soil carbon and nitrogen cycles. I. Modeling scheme. *Advances in Water Resources*, 26(1), 45–58. [https://doi.org/10.1016/S0309-1708\(02\)00094-5](https://doi.org/10.1016/S0309-1708(02)00094-5)
- Porporato, A., Laio, F., Ridolfi, L., Caylor, K. K., & Rodriguez-Iturbe, I. (2003). Soil moisture and plant stress dynamics along the kalahari precipitation gradient: Kalahari soil moisture and dynamical plant stress. *Journal of Geophysical Research*, 108(D3). <https://doi.org/10.1029/2002JD002448>
- Porporato, A., & Yin, J. (2022). *Ecohydrology: Dynamics of life and water in the critical zone*. Cambridge university press.
- Reershemius, T., Kelland, M. E., Jordan, J. S., Davis, I. R., D'Ascanio, R., Kalderon-Asael, B., et al. (2023). Initial validation of a soil-based mass-balance approach for empirical monitoring of enhanced rock weathering rates. *Environmental Science & Technology*, 57(48), 19497–19507. <https://doi.org/10.1021/acs.est.3c03609>
- Renforth, P. (2012). The potential of enhanced weathering in the UK. *International Journal of Greenhouse Gas Control*, 10, 229–243. <https://doi.org/10.1016/j.ijggc.2012.06.011>

- Renforth, P., & Henderson, G. (2017). Assessing ocean alkalinity for carbon sequestration. *Reviews of Geophysics*, 55(3), 636–674. <https://doi.org/10.1002/2016RG000533>
- Renforth, P., Pogge von Strandmann, P., & Henderson, G. (2015). The dissolution of olivine added to soil: Implications for enhanced weathering. *Applied Geochemistry*, 61, 109–118. <https://doi.org/10.1016/j.apgeochem.2015.05.016>
- Rodríguez-Iturbe, I., D'Odorico, P., Porporato, A., & Ridolfi, L. (1999). Tree-grass coexistence in Savannas: The role of spatial dynamics and climate fluctuations. *Geophysical Research Letters*, 26(2), 247–250. <https://doi.org/10.1029/1998GL900296>
- Schabernack, J., & Fischer, C. (2022). Improved kinetics for mineral dissolution reactions in pore-scale reactive transport modeling. *Geochimica et Cosmochimica Acta*, 334, 99–118. <https://doi.org/10.1016/j.gca.2022.08.003>
- Schaller, J., Puppe, D., Kaczorek, D., Ellerbrock, R., & Sommer, M. (2021). Silicon cycling in soils revisited. *Plants*, 10(2), 295. <https://doi.org/10.3390/plants10020295>
- Strefler, J., Amann, T., Bauer, N., Kriegler, E., & Hartmann, J. (2018). Potential and costs of carbon dioxide removal by enhanced weathering of rocks. *Environmental Research Letters*, 13(3), 034010. <https://doi.org/10.1088/1748-9326/aaa9c4>
- Stumm, W., & Morgan, J. J. (1996). *Aquatic chemistry: Chemical equilibria and rates in natural waters* (3rd ed. ed.). Wiley.
- Taylor, L. L., Driscoll, C. T., Groffman, P. M., Rau, G. H., Blum, J. D., & Beerling, D. J. (2021). Increased carbon capture by a silicate-treated forested watershed affected by acid deposition. *Biogeosciences*, 18(1), 169–188. <https://doi.org/10.5194/bg-18-169-2021>
- Taylor, L. L., Quirk, J., Thorley, R. M. S., Kharecha, P. A., Hansen, J., Ridgwell, A., et al. (2016). Enhanced weathering strategies for stabilizing climate and averting ocean acidification. *Nature Climate Change*, 6(4), 402–406. <https://doi.org/10.1038/nclimate2882>
- te Pas, E. E. E. M., Hagens, M., & Comans, R. N. J. (2023). Assessment of the enhanced weathering potential of different silicate minerals to improve soil quality and sequester CO₂. *Frontiers in Climate*, 4. <https://doi.org/10.3389/fclim.2022.954064>
- Val Martin, M., Blanc-Betes, E., Fung, K. M., Kantzas, E. P., Kantola, I. B., Chiaravalloti, I., et al. (2023). Improving nitrogen cycling in a land surface model (CLM5) to quantify soil N₂O, NO, and NH₃ emissions from enhanced rock weathering with croplands. *Geoscientific Model Development*, 16(20), 5783–5801. <https://doi.org/10.5194/gmd-16-5783-2023>
- Vienne, A., Poblador, S., Portillo-Estrada, M., Hartmann, J., Ijehon, S., Wade, P., & Vicca, S. (2022). Enhanced weathering using basalt rock powder: Carbon sequestration, Co-benefits and risks in a mesocosm study with *Solanum tuberosum*. *Frontiers in Climate*, 4. <https://doi.org/10.3389/fclim.2022.869456>
- Vries, W. d., & Posch, M. (2003). *Derivation of cation exchange constants for sand, loess, clay and peat soils on the basis of field measurements in The Netherlands* (Tech. Rep. No. 701). Alterra. Retrieved from <https://library.wur.nl/WebQuery/wurpubs/349403/ISSN:1566-7197>
- Wang, J. J., Dodla, S. K., & Henderson, R. E. (2004). Soil silicon extractability with seven selected extractants in relation to colorimetric and ICP determination. *Soil Science*, 169(12), 861–870. <https://doi.org/10.1097/00010694-200412000-00005>
- Weil, R. R., & Brady, N. (2016). *The nature and properties of soils* (15th ed.). Pearson.
- Wieder, W. R., Bonan, G. B., & Allison, S. D. (2013). Global soil carbon projections are improved by modelling microbial processes. *Nature Climate Change*, 3(10), 909–912. <https://doi.org/10.1038/nclimate1951>
- Wolf-Gladrow, D. A., Zeebe, R. E., Klaas, C., Körtzinger, A., & Dickson, A. G. (2007). Total alkalinity: The explicit conservative expression and its application to biogeochemical processes. *Marine Chemistry*, 14.
- Zhang, S., Planavsky, N. J., Katchinoff, J., Raymond, P. A., Kanzaki, Y., Reershemius, T., & Reinhard, C. T. (2022). River chemistry constraints on the carbon capture potential of surficial enhanced rock weathering. *Limnology & Oceanography*, 67(S2), S148–S157. <https://doi.org/10.1002/lno.12244>

Erratum

Since original publication of this article, the following has been added to the Acknowledgments: “L.V.N. acknowledges support by European Union NextGenerationEU – National Recovery and Resilience Plan (PNRR), Mission 4, Component 2, PRIN 2022 PNRR P20225K9YW – CUP B53D23033470001.” This may be considered the authoritative version of record.